COMPARISON OF NOAA/AVHRR AND LANDSAT/TM DATA IN TERMS OF RESEARCH APPLICATIONS ON THERMAL CONDITIONS IN URBAN AREAS

Monika J. Hajto[1]*, Jakub P. Walawender[2,3] and Piotr Struzik[2]

[1] Department of Air Pollution Monitoring and Modelling, Institute of Meteorology and Water Management – National Research Institute (IMGW-PIB), 14 Borowego St., PL-30215, Krakow, Poland
* monika.hajto@imgw.pl
[2] Satellite Remote Sensing Centre, Institute of Meteorology and Water Management – National Research Institute (IMGW-PIB), 14 Borowego St., PL-30215, Krakow, Poland
[3] Department of Climatology, Institute of Geography and Spatial Management, Jagiellonian University, 7 Gronostajowa St., PL-30387, Krakow, Poland

Abstract

This comparative case study examines land surface temperature (LST) maps derived from NOAA/AVHRR and LANDSAT/TM thermal infrared (TIR) data. Their spatial resolution is respectively 1.09 km and 120 m. NOAA/AVHRR satellite images are available for the same area up to several times a day, LANDSAT/TM images – at interval of 16 days. In this study NOAA-17/AVHRR and LANDSAT-5/TM images recorded on July 22nd, 2007 at about 9:30 UTC were used. The study area was the city of Krakow (Poland) and its surroundings. In order to retrieve the LST values Ulivieri et al. (1994) split-window algorithm for NOAA/AVHRR and Jiménez-Muñoz and Sobrino (2003) single-channel algorithm for LANDSAT/TM were applied. Land surface emissivity (LSE) included in the algorithms was estimated by Normalized Difference Vegetation Index Thresholds Method ($NDVI^{THM}$). The NOAA/AVHRR-derived and LANDSAT/TM-derived LST maps showed similar thermal contrast within the study area – the highest values of LST correspond to built-up and industrial areas, the lowest ones to forest and other green areas. The LST maps were compared with each other by plotting raster cross-tabulation matrix to obtain LST difference map. 32.8 % of pixels with ± 1 °C difference between LST derived from NOAA/AVHRR and LANDSAT/TM appeared. Comparison of LST maps included also drawing across them two profiles (WSW-ENE and NW-SE). They resulted similar courses in general, exactly their tendencies. Furthermore, on the basis of land use/land cover (LULC) map zonal statistics were computed for NOAA/AVHRR and LANDSAT/TM LST maps. In both cases industrial zones were recognised as the warmest LULC types while urban fabric was slightly less warm, and the coldest ones were forests and green urban areas. Results suggest the comparability of applied methods of estimating LST using different satellite data.

INTRODUCTION

Satellite remote sensing provides valuable data for investigation of urban climate characteristics such as urban heat island (UHI). Land surface temperature (LST) values retrieved from remotely sensed thermal infrared (TIR) images are one of the more and more used sources of information about UHI spatial patterns. Satellite radiometers, however, differ in spatial and temporal resolution of recorded images as well as number of spectral channels in TIR. Different technical properties of satellite systems influence applicability of satellite data for urban climate research (Tomlinson et al., 2011; Voogt and Oke, 2003; Weng, 2009).

The objective of this study is to compare land surface temperature maps created on the basis of data obtained by two radiometers: AVHRR (Advanced Very High Resolution Radiometer) onboard NOAA satellites and TM (Thematic Mapper) onboard LANDSAT-5 satellite. The first instrument records images in 1.09km spatial resolution, up to several times a day in two TIR channels. The second one provides images in higher spatial resolution 120m only in one TIR channel but at interval of 16 days.

Comparative case study for NOAA-17/AVHRR and LANDSAT-5/TM images obtained on July 22nd, 2007 was done. On that day both radiometers scanned area of the city of Krakow (Southern Poland) almost exactly at the same time (about 9:30 UTC).

Two most commonly used methods were applied in order to retrieve the LST values: Split-Window Algorithm for NOAA/AVHRR and Single-Channel Algorithm for LANDSAT/TM. The algorithms are very

different but both of them include correction of atmospheric influences on the measurements and emissivity effects. These are the most important steps of the LST retrieval procedure especially as far as comparison analysis is concerned.
The comparative analysis of the LST maps performed was to determine differences between the NOAA/AVHRR-derived and the LANDSAT/TM-derived LST values in the whole study area and along the profiles drawn across it. Furthermore, in both cases dependence of LST on land use/land cover (LULC) type was defined calculating basic zonal statistics taking as zones 6 generalised LULC types.
General recommendation on the use of NOAA/AVHRR and LANDSAT/TM images for urban climate research is presented.

STUDY AREA

The study area is the city of Krakow with its surroundings. It is situated in Southern Poland in varied terrain (Fig. 1 a-b). The Krakow city is located in the Vistula river valley. Its area within the administrative border is 326.8 km^2. Population of Krakow is over 750 000.
The study area contains land use/land cover (LULC) types such as urban fabric, industrial zones, arable lands, other agricultural areas, forests and urban green areas, and waters (Fig. 2).
Krakow urban climate is characterised by phenomenon of UHI with maximal temperature values around the city centre and the steelworks area in the eastern part of Krakow (Walawender and Hajto, 2009). Due to specific location of Krakow ventilation conditions are weakened resulting in problems with air pollution.

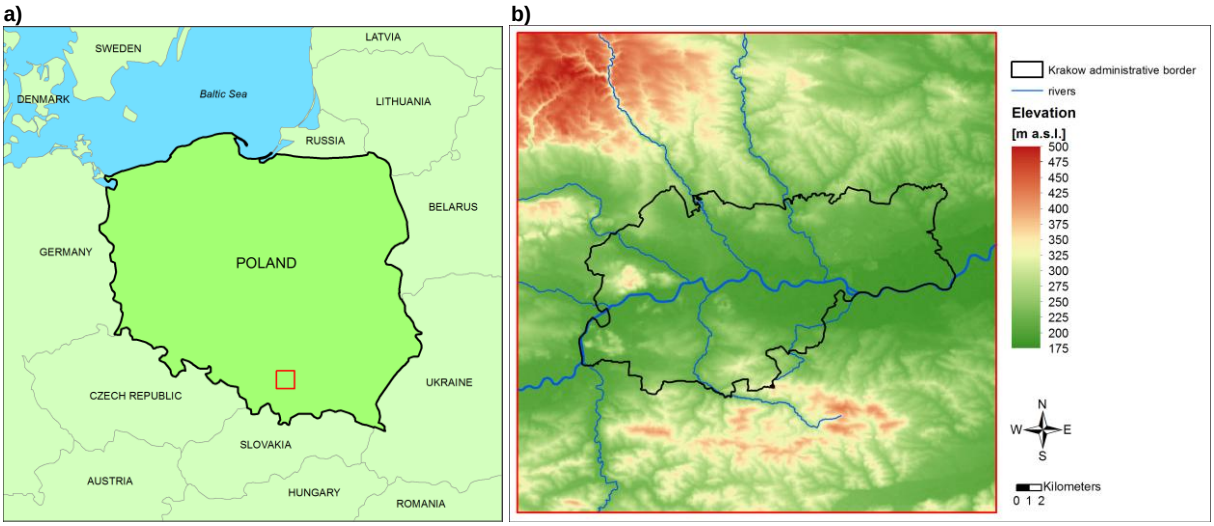

Figure 1: **Location of the study area (Krakow, Poland): a) marked as a red rectangle on the map representing the borders of Poland and neighbouring European countries; b) terrain map with the city administrative border**

DATA AND METHODS

Satellite images

NOAA-17/AVHRR and LANDSAT-5/TM images recorded on July 22nd, 2007 at about 9:30 UTC were used. Characteristics of TIR data from the satellite sensors are presented (Tab. 1). Maps of NOAA/AVHRR-derived and LANDSAT/TM-derived LST were made.

Satellite sensor	Wavelength range of TIR channel [µm]	Spatial resolution of TIR data [m x m]
NOAA/AVHRR	channel 4: 10.3-11.3 channel 5: 11.5-12.5	1090 x 1090
LANDSAT/TM	channel 6: 10.4-12.5	120 x 120

Table 1: **Wavelength ranges of thermal infrared (TIR) channels and spatial resolution of TIR data from the satellite sensors**

Land Surface Temperature (LST) retrieval

1. Radiometric calibration

At-sensor spectral radiance (L_λ) is acquired using digital numbers (*DN*) of TIR image and specified radiometric calibration coefficients *g* (slope/gain) and *b* (intercept/bias) according to $L_\lambda = g \cdot DN + b$ (for NOAA/AVHRR further non-linear correction is required).

At-sensor brightness temperature (T_λ) can be obtained from inversion of Planck's law according to:

$$T_\lambda = \frac{c_2}{\lambda \ln\left(\frac{c_1}{\lambda^5 L_\lambda} + 1\right)}$$

where c_1 and c_2 are the Planck's radiation constants ($c_1 = 1.19104 \cdot 10^8$ W · μm^4 · m^{-2} · sr^{-1} and $c_2 = 1.43877 \cdot 10^4$ μm · K), λ is effective wavelength of TIR channel.

2. Split-Window Algorithm for NOAA/AVHRR

With the use of brightness temperature values from NOAA/AVHRR TIR channels 4 and 5 LST is calculated by the split-window method. The recommended LST split-window algorithm proposed by Ulivieri et al. (1994) is applied (Pozo Vázquez et al., 1997; Qin et al., 2004):

$$LST = T_{\lambda i} + 1.8\left(T_{\lambda i} - T_{\lambda j}\right) + 48\left(1 - \varepsilon\right) - 75\Delta\varepsilon$$

where *i* and *j* are NOAA/AVHRR TIR channels 4 and 5, ε is land surface emissivity (LSE) which means the average value for NOAA/AVHRR TIR channels: $\varepsilon = (\varepsilon_{\lambda i} + \varepsilon_{\lambda j})/2$ and $\Delta\varepsilon = \varepsilon_{\lambda i} - \varepsilon_{\lambda j}$.

By means of the split-window method correction of atmospheric effects is made.

3. Single-Channel Algorithm for LANDSAT/TM

Using spectral radiance and brightness temperature values from LANDSAT/TM TIR channel 6 LST is calculated by the single-channel algorithm (Jiménez-Muñoz and Sobrino, 2003; Sobrino et al., 2004; Jiménez-Muñoz et al., 2009; Cristóbal et al., 2009):

$$LST = \left\{\frac{c_2 L_\lambda}{T_\lambda^2}\left[\frac{\lambda^4 L_\lambda}{c_1} + \frac{1}{\lambda}\right]\right\}^{-1} \left\{\left[\frac{1}{\varepsilon}(\psi_1 L_\lambda + \psi_2) + \psi_3\right] - L_\lambda\right\} + T_\lambda$$

where ε is the land surface emissivity (LSE) for LANDSAT/TM TIR channel, ψ_1, ψ_2 and ψ_3 are the atmospheric functions (AFs) defined as:

$$\psi_1 = \frac{1}{\tau}; \qquad \psi_2 = -L^{\downarrow} - \frac{L^{\uparrow}}{\tau}; \qquad \psi_3 = L^{\downarrow}$$

with τ meaning atmospheric transmissivity, $L^{\uparrow}$ and $L^{\downarrow}$ as up-welling and down-welling atmospheric radiances. These parameters are calculated for specific site with the use of the online tool called Atmospheric Correction Parameter Calculator (Barsi et al., 2003, 2005). In this way correction of atmosphere influence is performed.

4. Land Surface Emissivity (LSE) estimation

LSE (ε_λ) for TIR channels of NOAA/AVHRR and LANDSAT/TM is estimated by Normalized Difference Vegetation Index Thresholds Method (NDVI^{THM}). NDVI is calculated according to equation:

$$NDVI = \frac{\rho_{NIR} - \rho_{VIS}}{\rho_{NIR} + \rho_{VIS}}$$

where ρ_{VIS} and ρ_{NIR} are reflectivity values of visible and near infrared channels (for NOAA/AVHRR channels 2 and 1, for LANDSAT/TM channels 4 and 3).

NDVI^{THM} uses certain NDVI values (thresholds) to distinguish between soil pixels (NDVI < NDVI$_S$), pixels of full vegetation (NDVI > NDVI$_V$) and mixed pixels (NDVI$_S$ ≤ NDVI ≤ NDVI$_V$), composed of soil and vegetation (Sobrino et al., 2008). Values of NDVI$_S$ = 0.2 and NDVI$_V$ = 0.5 are applied.

Emissivity of soil pixels (NDVI < 0.2) is set as $\varepsilon_\lambda = \varepsilon_{S\lambda}$ assuming bare soil emissivity ($\varepsilon_{S\lambda}$) 0.95 for NOAA/AVHRR channel 4, and 0.96 for NOAA/AVHRR channel 5 and for LANDSAT/TM channel 6.
Emissivity of full vegetation pixels (NDVI > 0.5) for NOAA/AVHRR and LANDSAT/TM TIR channels is set to 0.99 assuming typical vegetation emissivity ($\varepsilon_{V\lambda}$) 0.985, and correcting by C_λ which is a term that takes into account the cavity effect due to surface roughness (for full vegetation pixels $C_\lambda = 0.005$) according to equation $\varepsilon_\lambda = \varepsilon_{V\lambda} + C_\lambda$.
Emissivity of mixed pixels being a mixture of bare soil and vegetation is computed according to the formula (Sobrino et al., 2008): $\varepsilon_\lambda = \varepsilon_{V\lambda} \cdot P_v + \varepsilon_{S\lambda} \cdot (1 - P_v) + C_\lambda$ where: P_V is proportion of vegetation (fractional vegetation cover) which is derived from NDVI (Carlson and Ripley, 1997):

$$P_V = \left(\frac{NDVI - NDVI_S}{NDVI_V - NDVI_S} \right)^2$$

Table 2 includes summarised emissivity expressions for the NDVI thresholds adapted to the TIR channels of NOAA/AVHRR (4 and 5) and LANDSAT/TM (6).

Satellite sensor	NDVI<0.2	0.2≤NDVI≥0.5	NDVI>0.5
NOAA/AVHRR	$\varepsilon_4 = 0.95$ $\varepsilon_5 = 0.96$	$\varepsilon_4 = 0.968 + 0.021\ P_V$ $\varepsilon_5 = 0.974 + 0.015\ P_V$	$\varepsilon_4 = 0.99$ $\varepsilon_5 = 0.99$
LANDSAT/TM	$\varepsilon_6 = 0.96$	$\varepsilon_6 = 0.982 + 0.003\ P_V$	$\varepsilon_6 = 0.99$

Table 2: **Emissivity expressions for the NDVI thresholds adapted to the satellite sensors (Sobrino et al., 2008)**

LST difference map

The NOAA/AVHRR-derived and LANDSAT/TM-derived LST maps were compared with each other by plotting raster cross-tabulation matrix. As a result a map of LST difference was obtained.

LST profiles

Comparison of LST maps included also drawing across them two profiles: Profile 1 (WSW-ENE) and Profile 2 (NW-SE) (Fig. 2).

Land use/land cover (LULC) map

On the basis of LULC map zonal statistics were computed for both LST maps, where as zones were the following generalised LULC types: urban fabric, industrial zones, forests and green urban areas, arable lands, other agricultural areas, and waters (Fig. 2).

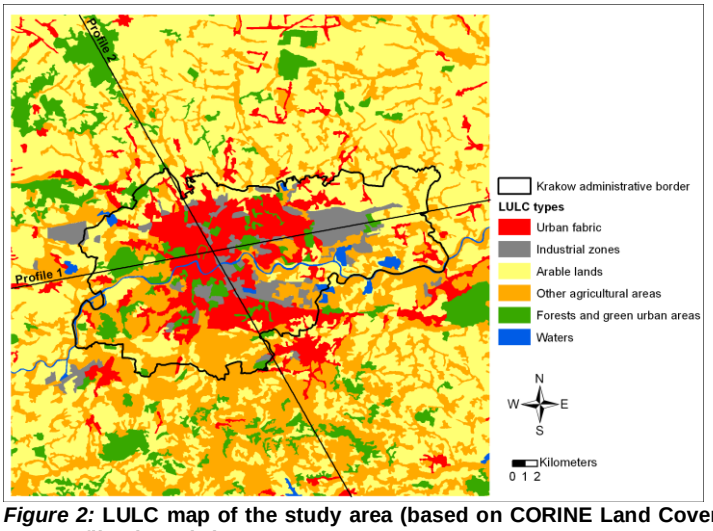

Figure 2: **LULC map of the study area (based on CORINE Land Cover 2006 data); crossing lines represent courses of LST profiles (1 and 2)**

RESULTS

LST maps

NOAA/AVHRR-derived and LANDSAT/TM-derived LST maps (Fig. 3 and Fig. 4) shows similar thermal contrast within the study area (Krakow and its surroundings). Pixels with higher values of LST particularly correspond to built-up and industrial areas. Forest and other green areas are noticeably colder. LST average value of all pixels covering the study area in both cases is 35.1 °C. LST derived from LANDSAT/TM reaches significantly higher maximal values (up to 62.5 °C, while for NOAA/AVHRR it is 43.8 °C) and lower minimal values (down to 25.3 °C while for NOAA/AVHRR it is 28.7 °C).

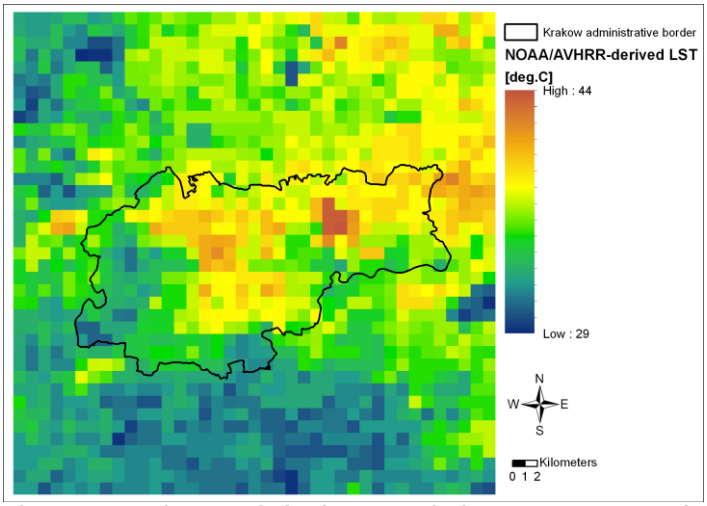

Figure 3: **NOAA/AVHRR-derived LST map (July 22, 2007, 09:31 UTC)**

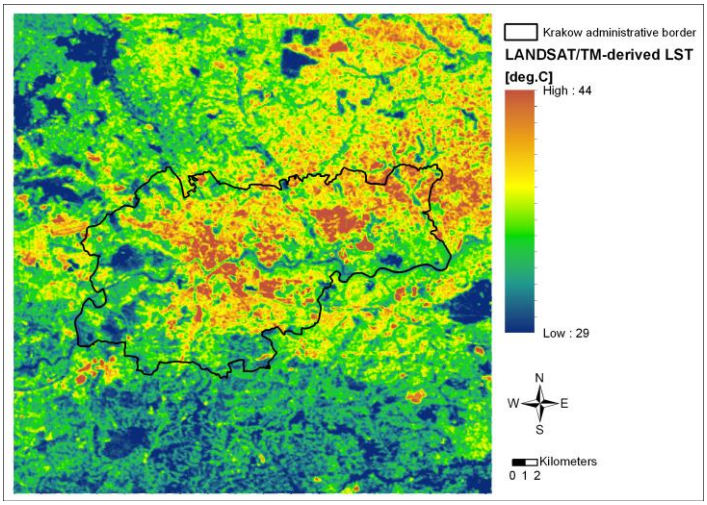

Figure 4: **LANDSAT/TM-derived LST map (July 22, 2007, 09:33 UTC)**

Comparative analysis of LST maps

Map of LST difference (Fig. 5) shows 32.8 % of pixels with difference between LST derived from NOAA/AVHRR and LANDSAT/TM which do not exceed ± 1 °C. Greater LST differences occur equally in plus and in minus, respectively for 33.5 % and 33.7 % of pixels.

LST profiles (Fig. 6 a-b) drawn across NOAA/AVHRR-derived and LANDSAT/TM-derived maps resulted similar courses in general, exactly their tendencies. Changes of each course are referring to LULC types.

LST dependence on LULC

Basic zonal statistics calculated based on LULC map for NOAA/AVHRR-derived and LANDSAT/TM-derived LST maps (Fig. 7 a-b) show similar dependencies. In both cases the warmest LULC types are

industrial zones. Urban fabric is slightly less warm LULC type. Forests and green urban areas are the coldest LULC types both for NOAA/AVHRR and LANDSAT/TM LST maps. Ranges of LST values for each LULC type are obviously greater in case of LANDSAT/TM map.

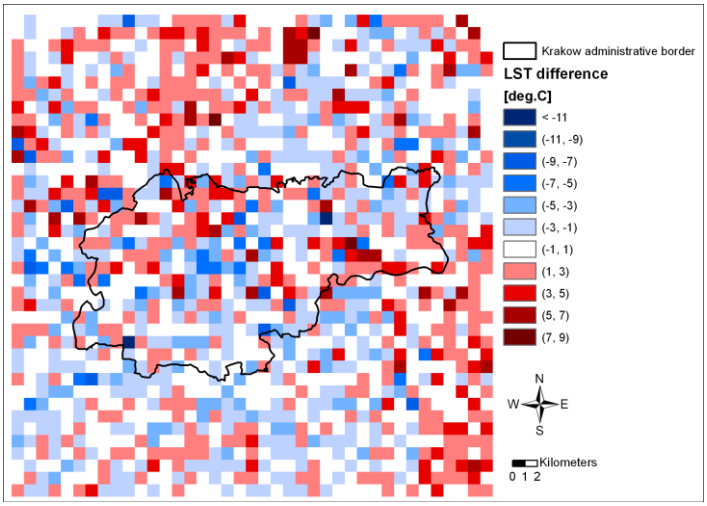

Figure 5: **Map of LST difference between NOAA/AVHRR-derived LST map and LANDSAT/TM-derived LST map**

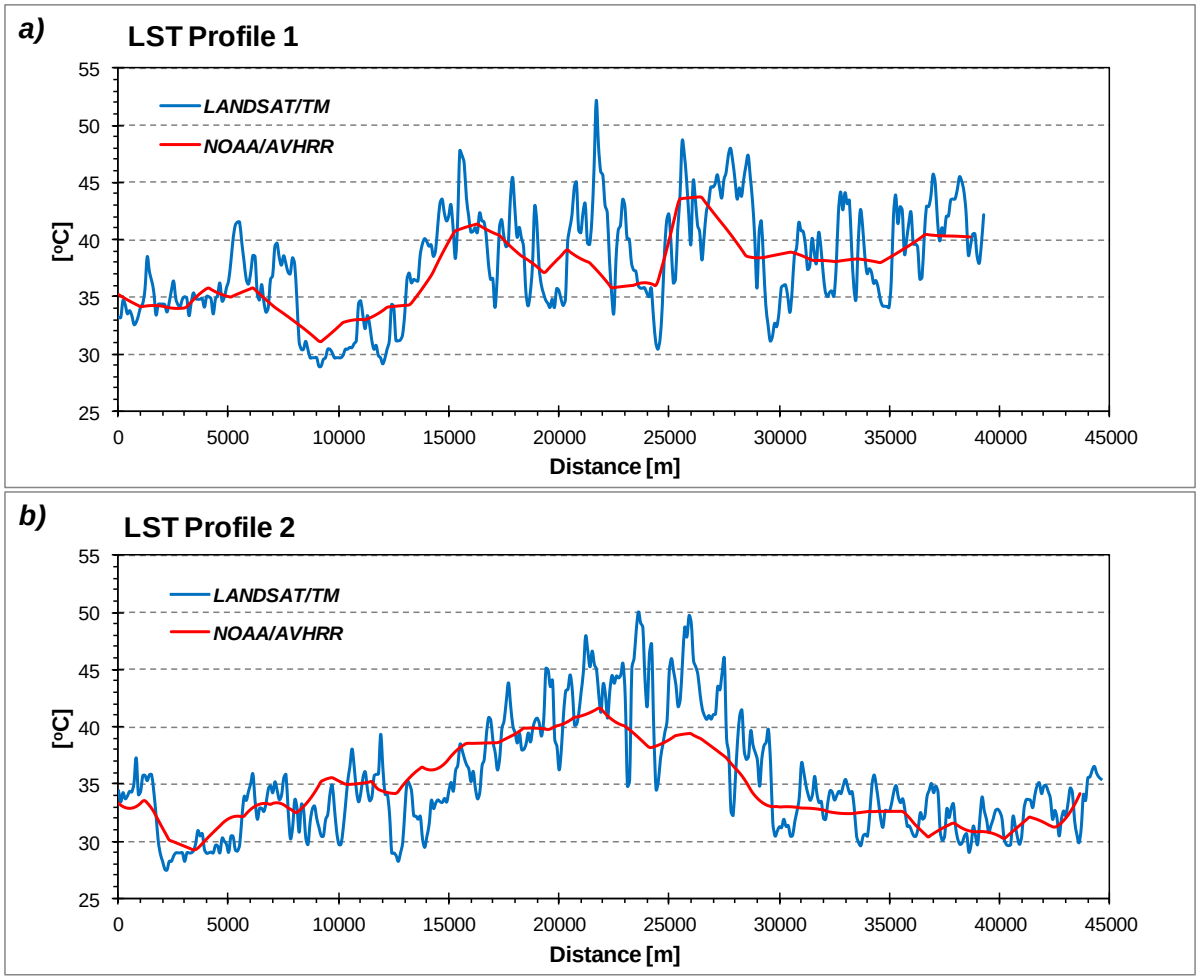

Figure 6: **Comparison of LST profiles obtained from NOAA/AVHRR-derived and LANDSAT/TM-derived LST maps; a) Profile 1 (WSW-ENE); b) Profile 2 (NW-SE)**

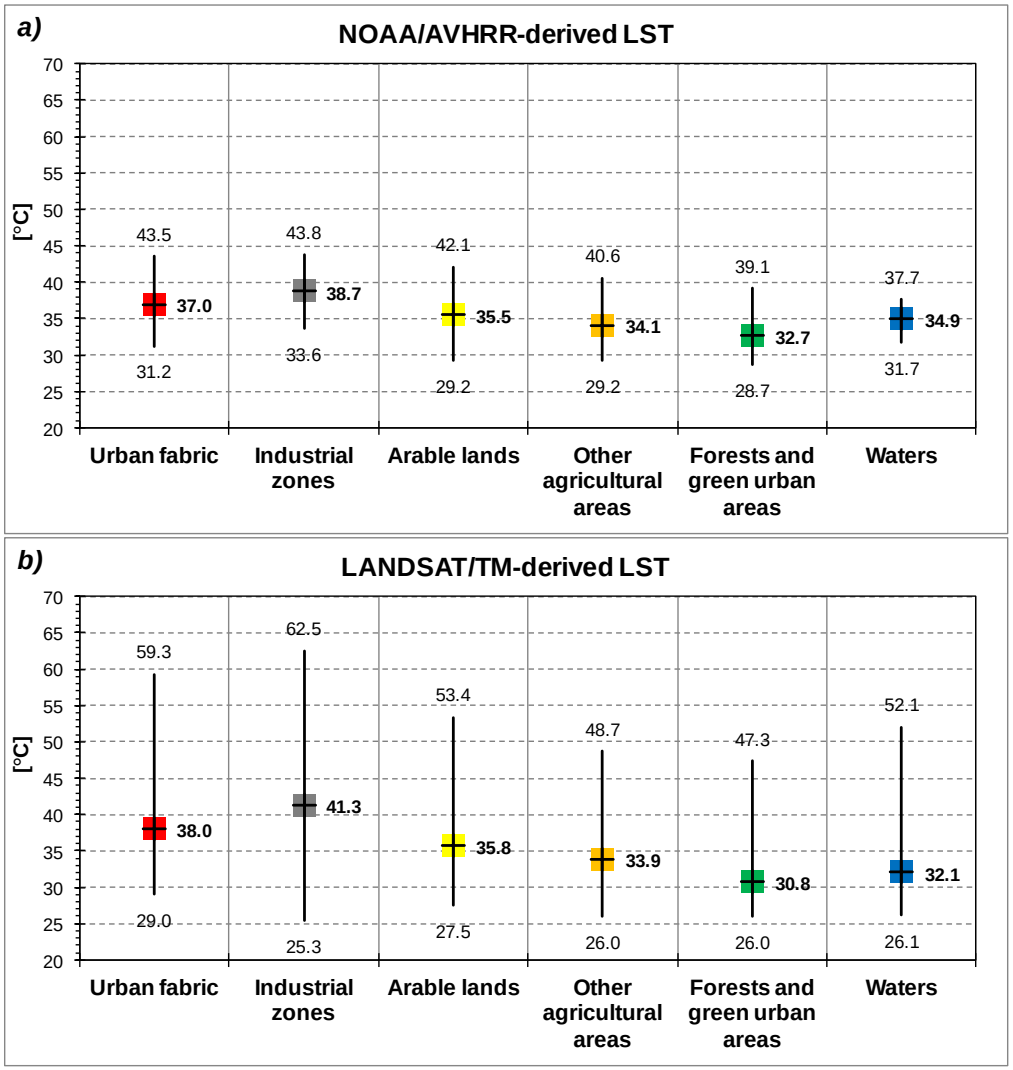

Figure 7: **Mean, maximal and minimal values of NOAA/AVHRR-derived (a) and LANDSAT/TM-derived (b) LST calculated for different LULC types**

CONCLUSIONS

Results of this case study suggest the comparability of applied methods of estimating LST using different satellite data. This would give a basis for integration of NOAA/AVHRR and LANDSAT/TM data in terms of monitoring spatio-temporal changes of LST in urban areas. Therefore, downscaling of 1 km LST map to 120 m spatial resolution seems to be reasonable. Relatively high spatial resolution of LANDSAT/TM data allows for more accurate spatial analyses while great temporal resolution of NOAA/AVHRR enables investigating diurnal changeability of LST spatial patterns (Hajto et al., 2012).
Automated LST computations by means of GIS tools that was applied for LANDSAT/TM data (Walawender et al., 2012) may improve processing of data from different satellite radiometers. LST maps acquired in this way can be then analysed in GIS software environment.
LST maps could be used in mesoscale meteorological models such as MM5 or WRF, especially for heat fluxes determination.

Acknowledgements

NOAA/AVHRR data taken from IMGW-PIB Satellite Receiving Station archive. VCS 2Met! software was used for radiometric calibration and geometric correction of NOAA/AVHRR data. LANDSAT/TM data taken from U.S. Geological Survey archive (http://glovis.usgs.gov). ESRI ArcGIS Desktop 10 software was used for visualisation and spatial analyses. Generalised LULC map was performed with the use of CORINE Land Cover 2006 data. The research was performed with the financial support of The National Centre for Research and Development of Poland (project no. NR14-0013-10/2010).

REFERENCES

Barsi, J. A., J.L. Barker and Schott J. R., (2003). An Atmospheric Correction Parameter Calculator for a Single Thermal Band Earth-Sensing Instrument. In *Proceedings of IEEE International Geoscience And Remote Sensing Symposium (IGARSS)*, Toulouse, France, July 21-25.

Barsi, J. A., J. R. Schott, F. D. Palluconi and S. J. Hook, (2005). Validation of a Web-Based Atmospheric Correction Tool for Single Thermal Band Instruments. In *Earth Observing Systems X. Proceedings of SPIE* (ed. J. J. Butler), **5882**, Bellingham, WA, USA.

Carlson, T. N., and D. A. Ripley, (1997).On the relation between NDVI, fractional vegetation cover and leaf area index. *Remote Sensing of Environment*, **62 (3)**: p. 241-252.

Cristóbal, J., J. C. Jiménez-Muñoz, J. A. Sobrino, M. Ninyerola and X. Pons, (2009). Improvements in land surface temperature retrieval from the Landsat series thermal band using water vapour and air temperature. *Journal of Geophysical Research*, **114**, D08103. doi: 10.1029/2008JD010616.

Hajto, M. J., J. P. Walawender and P. Struzik, (2012). Spatio-temporal changes of land surface temperature in Krakow (Poland) determined using NOAA/AVHRR data. In *Proceedings of 8th International Conference on Urban Climate (ICUC8).* Dublin, Ireland, August 6-10.

Jiménez-Muñoz, J. C., J. Cristóbal, J. A. Sobrino, G. Sòria, M. Ninyerola and X. Pons, (2009). Revision of the Single-Channel Algorithm for Land Surface Temperature Retrieval From Landsat Thermal-Infrared Data. *IEEE Transactions on Geoscience and Remote Sensing*, **47 (1)**: p. 339-349. doi: 10.1109/TGRS.2008.2007125.

Jiménez-Muñoz, J. C., and J. A. Sobrino, (2003). A generalized single-channel method for retrieving land surface temperature from remote sensing data. *Journal of Geophysical Research*, **108**, 4688. doi: 10.1029/2003JD003480.

Pozo Vázquez, D., F. J. Olmo Reyes and L. Alados Arboledas, (1997). A comparative study of algorithms for estimating land surface temperature from AVHRR data. *Remote Sensing of Environment*, **62**: p. 215-222.

Qin, Z., B. Xu, W. Zhang, W. Li and H. Zhang, (2004). Comparison of split window algorithms for land surface temperature retrieval from NOAA-AVHRR data. In *Proceedings of 2004 IEEE International Geoscience And Remote Sensing Symposium (IGARSS)*, **6**: p. 3740-3743. Anchorage, AK, USA, September 20-24.

Sobrino, J. A., J. C. Jiménez-Muñoz and L. Paolini, (2004). Land surface temperature retrieval from Landsat TM 5. *Remote Sensing of Environment*, **90 (4)**: p. 434-440.

Sobrino, J. A., J. C. Jiménez-Muñoz, G. Sòria, M. Romaguera, L. Guanter, J. Moreno, A. Plaza and P. Martínez, (2008). Land surface emissivity retrieval from different VNIR and TIR sensors. *IEEE Transactions on Geoscience and Remote Sensing*, **46 (2)**: p. 316-327. doi:10.1109/TGRS.2007.904834.

Tomlinson, C. J., L. Chapman, J. E. Thornes, and C. Baker, (2011). Remote sensing land surface temperature for meteorology and climatology: a review. *Meteorological Applications*, **18**: p. 296-306.

Ulivieri, C., M. M. Castronuovo, R. Francioni and A. Cardillo, (1994). A split-window algorithm for estimating land surface temperature from satellites. *Advances in Space Research*, **14**: p. 59-65.

Voogt, J. A., and T. R. Oke, (2003). Thermal remote sensing of urban climates. *Remote Sensing of Environment*, **86**: p. 370-384.

Walawender, J., and M. Hajto, (2009). Assessment of thermal conditions in urban areas with use of different satellite data and GIS. In *Proceedings of 2009 EUMETSAT Meteorological Satellite Conference*. Bath, United Kingdom, September 21-25.

Walawender, J. P., M. J. Hajto, and P. Iwaniuk, (2012). A new ArcGIS toolset for automated mapping of land surface temperature with the use of LANDSAT satellite data. In *Proceedings of IEEE International Geoscience And Remote Sensing Symposium (IGARSS)*. Munich, Germany, 22-27 July.

Weng, Q., (2009). Thermal infrared remote sensing for urban climate and environmental studies: Methods, applications, and trends. *ISPRS Journal of Photogrammetry and Remote Sensing*, **64**: p. 335-344.